Progress in beam focusing and compression for warm-dense matter experiments

P.A. Seidl [a,*], A. Anders [a], F.M. Bieniosek [a], J.J. Barnard [b], J. Calanog [a,c], A.X. Chen [a,c], R.H. Cohen [b], J.E. Coleman [a,c], M. Dorf [d], E.P. Gilson [d], D.P. Grote [b], J.Y. Jung [a], M. Leitner [a], S.M. Lidia [a], B.G. Logan [a], P. Ni [a], P.K. Roy [a], K. Van den Bogert [a], W.L. Waldron [a], D.R. Welch [e]

[a] *Lawrence Berkeley National Laboratory, Berkeley, CA 94720, USA*
[b] *Lawrence Livermore National Laboratory, Livermore, CA 94550, USA*
[c] *University of California, Berkeley, CA 94720, USA*
[d] *Princeton Plasma Physics Laboratory, Princeton, NJ 08543-0451, USA*
[e] *Voss Scientific, Albuquerque, NM 87108, USA*

ARTICLE INFO

ABSTRACT

The Heavy-Ion Fusion Sciences Virtual National Laboratory is pursuing an approach to target heating experiments in the warm-dense matter regime, using space-charge-dominated ion beams that are simultaneously longitudinally bunched and transversely focused. Longitudinal beam compression by large factors has been demonstrated in the Neutralized Drift Compression Experiment (NDCX) with controlled ramps and forced neutralization. Using an injected 30-mA K^+ ion beam with initial kinetic energy 0.3 MeV, axial compression leading to ~50-fold current amplification and simultaneous radial focusing to beam radii of a few mm have led to encouraging energy deposition approaching the intensities required for eV-range target heating experiments. We discuss the status of several improvements to our Neutralized Drift Compression Experiment and associated beam diagnostics that are under development to reach the necessary higher beam intensities, including (1) greater axial compression via a longer velocity ramp using a new bunching module with approximately twice the available volt seconds (Vs); (2) improved centroid control via beam steering dipoles to mitigate aberrations in the bunching module; (3) time-dependent focusing elements to correct considerable chromatic aberrations; and (4) plasma injection improvements to establish a plasma density always greater than the beam density, expected to be $> 10^{13} \, \mathrm{cm}^{-3}$.

1. Introduction

To create a short (~ns) pulse with duration suitable for the study of warm-dense matter [1], our approach has been to modulate the energy of an initially much-longer non-relativistic beam. To achieve target temperatures around ~1 eV, the required beam intensity necessitates space-charge neutralization, which has been achieved with a background plasma through which the beam passes while it is focusing transversely and bunching longitudinally.

We are approaching the required beam intensities for heating targets toward warm-dense matter conditions, and have arrived at this stage through a sequence of experiments over the past several years. The scaled final focusing experiment demonstrated the successful neutralization of an initially space-charge-dominated beam by a background source of electrons in order to achieve an emittance-limited focal spot [2]. The experiment was scaled from a design of a final focusing system for a heavy-ion fusion driver using quadrupole magnets for beam transport (driver parameters: 10 GeV Bi^+ at 1.25 kA/beam). Following initial experiments with an emittance-limited 95 μA, 160 keV Cs^+ beam, the beam current was then increased to 400 μA with a dimensionless perveance of $K = q\lambda (2\pi\varepsilon_0 mv^2) \approx 5 \times 10^{-5}$; space-charge limited near the focal plane for an unneutralized beam. The spot radius with neutralization was ~2× smaller than without, in agreement with models assuming 80% and 0% neutralization, respectively.

The Neutralized Transport Experiment (NTX), used a higher current (~25 mA) and higher energy (250–350 keV) K^+ beam. The beam perveance (~10^{-3}) was effectively neutralized with RF and cathodic-arc plasma sources [3]. This demonstrated the feasibility of neutralization of higher perveance beams and was a precursor to the additional feature of axial bunching of the ion beam.

The axial compression is achieved with an induction-bunching module (IBM) inserted after the matching section. Operating at

* Corresponding author. Tel./fax: +1 510 486 7653; fax: +1 510 486 5392.
E-mail address: PASeidl@lbl.gov (P.A. Seidl).

± 80 kV, a $\pm 12.5\%$ velocity ramp is imparted to 150–200 ns subset of the several-microsecond beam pulse. The beam then drifts through a neutralizing plasma in a drift compression section a few meters in length. Current amplification of ≈ 50 was demonstrated in the first NDCX experiments [4]. To establish a neutralizing plasma along most of the length of the drift compression section, the RF plasma used in NTX was replaced with a ferro-electric plasma source [5], and cathodic-arc plasma sources injected a high-density plasma near the focal plane where the beam density is greatest.

A fundamental limit to the current amplification and pulse duration is the longitudinal energy spread (longitudinal phase space and emittance) of the injected beam, as shown in Eq. (1):

$$t_{min} = \frac{L}{v^2}\sqrt{\frac{2kT}{M}}. \tag{1}$$

The quantity kT is the longitudinal temperature of the beam, M the ion mass, v the mean axial velocity of the ions, and L the drift compression distance. The energy spread was measured with an electrostatic energy analyzer (EEA) (Section 2.2). The measured energy spread is adequate for achieving nanosecond-duration bunches. Other limits are set by the uniformity and density of the background neutralizing plasma, and imperfections of the bunching module waveform. In general, simulations have shown that if the background plasma density is greater than the local beam density, then the effectiveness of the neutralization is independent of the details of the plasma density distribution [6]. For near-term warm-dense matter experiments, the beam density increases steeply and approaches $n_b = 10^{13}$ cm^{-3} near the target plane. We have measured plasma densities in that range with cathodic-arc plasma sources. The plasma temperature should be low enough to not heat the beam and we have found that plasma temperatures in the few eV range have a benign influence on the beam. In order to achieve the best transverse focusing and emittance-limited longitudinal compression, the background plasma density must exceed the local beam density. Depending on the beam and plasma densities, collective instabilities may limit the focused beam intensity, but for NDCX-I (based on both experiment and theory) and NDCX-II (based on theory) these instabilities appear to be benign.

In the induction-bunching module, radial electric fields are generated in the gap across which the IBM voltage is applied that includes a net radial defocusing effect on the bunching beam.

Following an analysis of this effect [7], it was determined that tuning the initial beam envelope to compensate for the defocusing of the IBM enabled simultaneous transverse focusing and axial compression [8], as shown in Section 2.5.

2. Results and discussion

We are studying and experimenting with a short, high-field solenoid ($B = 8$ T, 10-cm coil length) after the ferro-electric plasma source and before the target plane (see Fig. 1) to impart a steep convergence angle on the beam before the focal plane. LSP modeling suggests that sub-mm radii might be possible, leading to a several-fold increase in the peak energy deposition per unit area, assuming that a high plasma density can be injected into the bore of the solenoid [9]. A target chamber and new target heating diagnostics have been installed at the end of the beamline [10].

2.1. Beam diagnostics in the target chamber

An improved fast Faraday cup has been installed in the new target chamber (see Fig. 1). The basic design and operating principle is the same as described in Ref. [11] and the electronic response still allows for ≈ 1 ns resolution of the ion beam current. This is established mainly by the 1-mm gap between the suppressor plate and the collector, since the incoming ion ($v \approx 1.2$ m/µs) transit time of 1 ns will set the scale for the capacitive pickup of the ions approaching the collector. The new design enables variation of gaps between hole plates, and hole plate transparency, easier alignment of front hole plate to middle (bias) hole plate, and a metal enclosure for shielding from the background plasma and electronic noise. Each hole plate has a hexagonal array of holes, extending over a circular area with 30-mm diameter. In the current version, the front hole plate (held at ground potential) has 0.23 mm diameter holes spaced by 1 mm, while the middle hole plate (suppressor grid, biased to -75 V) has 0.46 mm diameter holes spaced by 1 mm. The holes are larger on the middle plate to prevent scraping. This 95-mrad tolerance between the concentric front plate holes and the middle plate holes should compensate for diverging ion trajectories and detector alignment imperfections. The collector plate is biased to $+75$ V. A schematic of this Faraday cup is shown in Fig. 2.
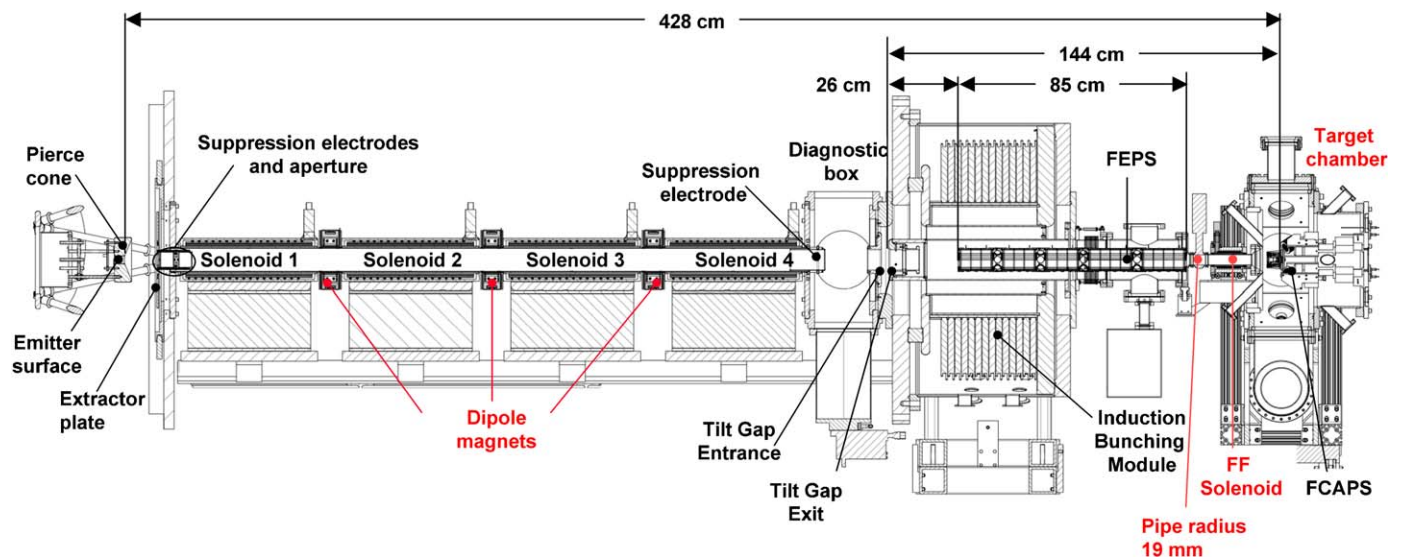

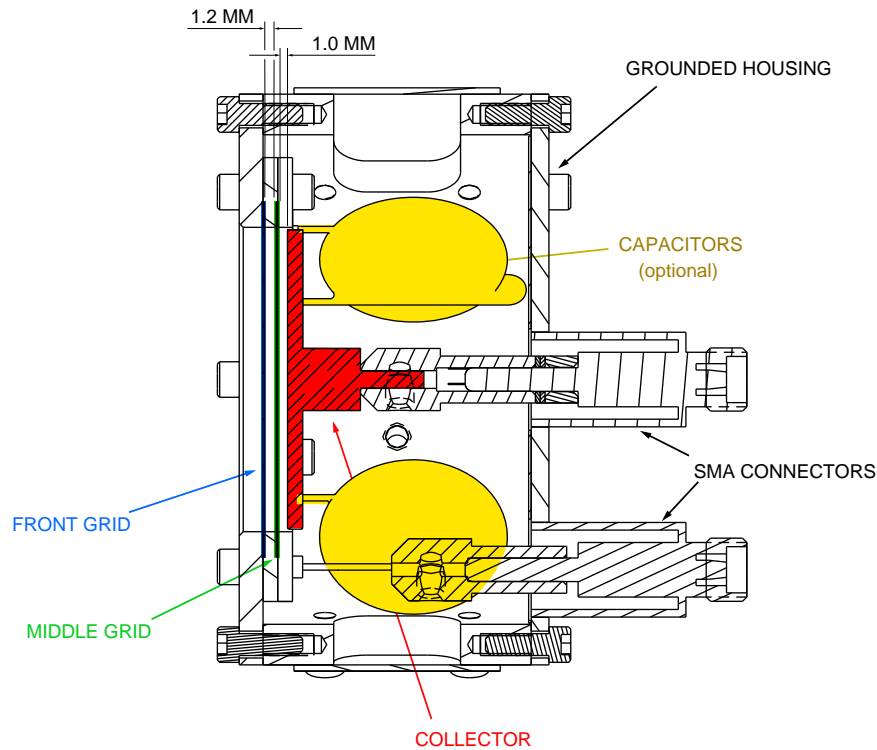**Fig. 1.** Elevation view of the Neutralized Drift Compression Experiment.
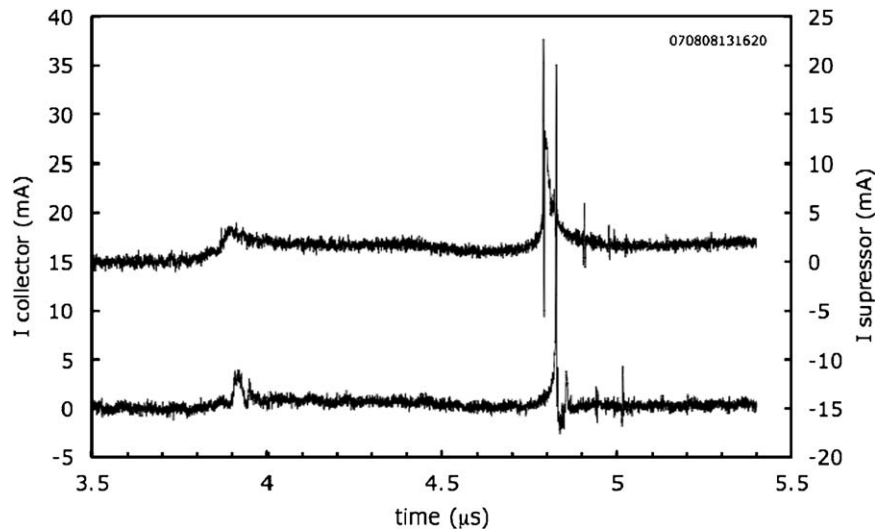
Fig. 2. Fast Faraday cup schematic.

Fig. 3. Faraday cup response to uncompressed beam and bunched portion ($t \approx 4.8\,\mu s$). The bottom trace is the collector electrode, and the top trace is the suppressor hole plate.

The geometric transparency of the front hole plate results in a reduction of the beam current reaching the collector grid by a factor of 44. Fig. 3 shows the response of the Faraday cup to the uncompressed head of the beam ($30\,mA\ K^+$, $1\,\mu s$ duration), and the compressed bunch at $t \approx 4.8\,\mu s$. The product of the collector signal amplitude and the hole plate transparency agrees ($\approx \pm 5\%$) with the upstream measurement of the beam current before the IBM. The suppressor signal has a similar response to the collector, and is not as well understood at this time. We are modeling the detector response with WARP [12] and LSP particle in cell simulations, including the effect of desorption and ionization of neutral atoms from the collector and front plate. The recognition of this latter effect as potentially significant is based on analytic

estimates using known desorption coefficients, charge-exchange cross-sections and ionization cross-sections. We are also studying possibility that ions are striking the middle plate due to detector misalignment, beam centroid misalignment, and large angle ion trajectories due to beam dynamics and also due to small angle scattering from the inside edge of the front plate holes. Simulations so far suggest that the plasma is effectively shielded by the front hole plate. The collector does, however, see significant plasma background from the cathodic-arc plasma sources. It is effectively a nearly flat, smoothly varying background and is subtracted during data analysis.

The transverse (spatial) distribution of the beam is measured by allowing the beam to strike a 100-µm thick alumina

scintillator, and then detecting the beam-induced light emission with an image-intensified-gated-MCP camera. The optical system produced a resolution of 10–17 pixels/mm (depending on the choice of lens and optics setup) at the image plane. Image acquisition and processing software are then used to collect and analyze the time-gated images of the beam [13]. A steel mesh of transparency 28% is placed on the upstream side of the scintillator. The relatively low transparency reduces the flux onto the scintillator and the degradation of the scintillator. It is biased to −300 V, creating a supply of electrons to discharge the scintillator caused by the accumulation of charge from the positive ion beam. Using a phototube, photodiode, and streak camera, the time dependence of the light output from the scintillator has been recorded to measure the compressed pulse duration independently of the fast Faraday cup.

2.2. Longitudinal phase space measurements

The energy spread, ΔE, of the non-relativistic ion beam is related to the longitudinal velocity spread Δv_z by $\Delta E = mv\Delta v_z$. Assuming the velocity distribution is a one-dimensional Maxwellian about the mean beam velocity, the temperature, T_z, of that distribution is given by

$$T_z = \frac{(\Delta E^2)}{2E_0}. \tag{2}$$

An electrostatic energy analyzer was placed at the exit of the ferro-electric plasma source, to measure the longitudinal phase space and energy spread of the uncompressed beam with and without plasma neutralization [14]. A special beam envelope tune was used for the un-neutralized beam to prevent particle loss in the 180-cm drift distance from the final matching solenoid to the entrance slit of the spectrometer. The entrance slit of the spectrometer was 0.1 mm × 5 mm, which allowed ~10 μA of the incident 30-mA K$^+$ beam to be transmitted through the spectrometer. The spectrometer is a 90° sector design with a bending radius of 75 cm and a gap of 2.5 cm between concentric dipole electrodes. The focal plane detectors were a moveable slit-Faraday cup and an alumina (Al$_2$O$_3$) scintillator with a CCD camera. For a 300 keV ion beam, deflection plate voltages were ±15 kV. The contribution of field quality to spectrometer resolution was estimated with ray tracing simulations through fields derived from the mechanical specifications of the field defining plates. The results suggest a resolution of $\Delta E/E \approx 5 \times 10^{-5}$, while the
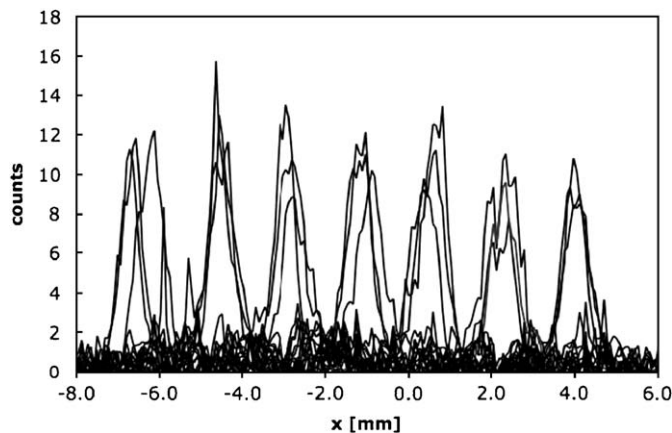
contribution from the 0.1 mm entrance slit gives a resolution of $\Delta E/E = 2 \times 10^{-4}$ or $\Delta E = 60$ eV. Thus, the choice of entrance slit width (motivated by detector signal-to-noise) is the dominant factor in determining the energy resolution for these data. The dispersion on the focal plane is 1.7 mm/keV and this is reflected in the data of Fig. 4, showing the profiles of a 500-ns slice of the beam subject to variations of the dipole plate voltages, for incident beam energy of 289 keV. The data were measured with the scintillator and image-intensified CCD camera. The entire energy acceptance of the spectrometer is displayed, about 7 keV. The variation among repeated shots (three per plate voltage setting) is indicative of the shot-to-shot energy variation of the beam, <0.1 keV (rms). The measured width of the distributions, or the energy spread of the injected $E_0 = 289$-keV un-bunched beam is $\Delta E \approx 0.17$ keV. The measured energy spread corresponds to an axial temperature of $T_z = 0.05$ eV, which is adequate for compressing the beam to <1 ns (Eq. (1)). Other mechanisms may limit the minimum pulse duration, such as incomplete neutralization of the compressed pulse, and waveform imperfections in the IBM.

No significant difference in the energy spread was observed between the neutralized and un-neutralized beam cases, suggesting minimal heating of the beam from the plasma. The time dependence of the energy distribution was recorded with a streak camera imaging the light emission from the scintillator (Fig. 5), and also with a slit-Faraday cup. The results reflect the slight decrease (2–4 kV/μs) of the injector Marx voltage after the initial rise to peak voltage. Signal-to-noise limitations obscured the detection of the acceleration of ions near the head of the beam due to longitudinal space charge. Particle-in-cell simulations suggested this would be a difficult signal to detect due to low signal amplitude.

2.3. Beam centroid control

Due to misalignments of the beamline components, the centroid betatron motion amplitude of a few mm manifested in an offset angle of several milliradians at the exit of the four matching solenoid lattice. Beam centroid corrections are required to minimize aberrations in IBM gap and for beam position control at the target plane.

Steering dipoles were designed to apply up to 20 mrad deflection to the 300 keV K$^+$ beam at each of the three gaps between the solenoids. The dipoles are composed of 39 turns of

Fig. 4. Beam image profiles as a function of focal plane position and deflection plate voltages. The incident beam energy was 289 keV, and the deflection plate voltages were scanned in 50-V steps around 14.5 kV (three shots at each step are shown), corresponding to beam energy variations of 1-keV steps.
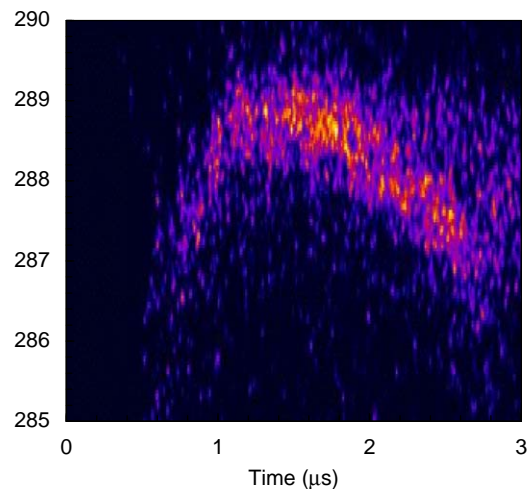

Fig. 5. Streak camera image of the longitudinal phase space of the uncompressed beam near the beginning of the pulse.

1-mm copper wire, in a uniform current density ($K(\theta) = $ constant for $-60 < \theta < 60°$) approximation to a $\cos(\theta)$ coil.

The horizontal and vertical deflection coils are nested and fit in the 0.1 m gap between solenoids and around the 100 mm diameter beam pipe. The coils are driven by capacitor discharge circuits with a pulse duration of 2 ms. A current of 100 A creates a dipole field of 0.05 T and a deflection to 0.3 MeV K^+ ions of ≈ 10 mrad. The steering solution was found by inversion of multiple sets of measurements of the beam centroid for different dipole currents. The linear assumption for the response yielded a much improved beam centroid without further iteration, indicating that the measurement uncertainty of 0.25 mm and 1 mrad were sufficiently accurate for a reliable inversion of the 4×4 Jacobian matrix. The results of steering are shown in Table 1. For this steering solution, only the second and third dipole sets were energized, with currents in the range of 56–194 A.

2.4. Plasma density measurements

The plasma density in the target chamber has been increased and now mostly exceeds the on-axis beam density to satisfy $n_p/n_b > 1$, where n_p and n_b are the plasma electron density and ion beam density, respectively. This work consists of several segments. First, the plasma density of two filtered cathodic-arc plasma sources (two-FCAPS) was measured with an axially moveable Langmuir probe with a 4-T solenoid magnetic field. Next, the two-FCAPS system was replaced by fabricating four cathodic-arc plasma sources (four-FCAPS) with straight filters (vs. the former 45° bend in the two-FCAPS system) to increase the plasma density. The solenoid magnetic field was increased to 8 T. Results show that the new four-FCAPS system, with the short straight filters and driven with a $3 \times$ higher discharge current provides 9–60 times greater plasma density than the two-FCAPS system with the bent filters. Assuming a plasma velocity of 2×10^4 m/s, the four-FCAPS system provided a peak plasma density 9×10^{12}–6×10^{13}/cm^3. Finally, the axial and radial plasma distribution was measured with a specially designed array of 37 Langmuir probes. These new data show that plasma forms a thin column of diameter ~5 mm along the solenoid axis when the final focus solenoid (FFS) is energized. The results are described in [15].

2.5. Beam compression and focusing results

A new 8-T pulsed final focus solenoid has been fabricated and installed at the target chamber entrance, and replaces the prototype solenoid that produced a 5-T peak field. The peak field of the first solenoid was limited by high-voltage flashover near the magnet leads and later was limited to 4 T peak field. The mechanical design and cooling system of the solenoid was improved, and the new solenoid consistently operates up to the design value of 8 T [15].

The Faraday cup in the diagnostic box has been used to measure the beam current transported to the entrance of the IBM. This measurement is used in a cross-normalization with the beam signal measured in the Target Chamber with the fast Faraday cup

Table 1
Results of optimization of beam steering using magnetic dipoles.

	$\langle x \rangle$ (mm)	$\langle x' \rangle$ (mrad)	$\langle y \rangle$ (mm)	$\langle y' \rangle$ (mrad)
Dipoles off	−5.81	2.24	−2.77	3.37
Dipoles on	−0.15	0.51	0.00	−0.31

First moments of the beam position and angle are measured at the exit of the four-solenoid matching section, just before the induction bunching module.
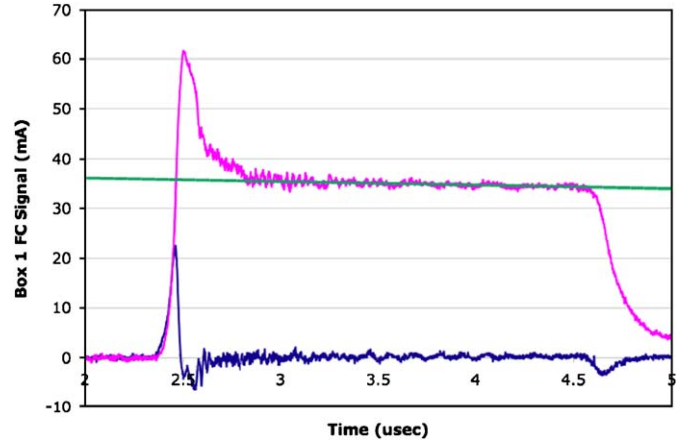

Fig. 6. Diagnostic box Faraday cup beam current measurements: the collector plate signal (top), the suppressor grid signal (bottom), and a linear fit to the collector signal flattop.

on a later pulse to establish the beam current and power impinging on the target plane.

An example of the measured Faraday cup response to the beam current generated during a 330 kV diode extraction is shown in Fig. 6. The linear fit to the flattop (green) shows the beam carrying 35.8 mA with a 0.7 mA/μs droop associated with the droop of the Marx voltage over this period. From this measure, the beam is delivering 11.8 mJ/μs beam power over the flattop region.

For a tune that optimizes the compressed beam fluence, the variation of spot radius with beam current (and power) is shown in Fig. 7. Here, the changes to the spot radius and transverse distribution are evident in this time scan across the compression peak. The peak beam current is 1.5 A. At peak compression, 50% of the beam flux is within a radius of 1.5 mm. The higher peak beam current was reported in [8], and the cause of the difference between the measurements is still being investigated. Topics under study include: diagnostic differences (new vs. old fast Faraday cup), detector alignment, IBM waveform fidelity, and plasma density differences. Meanwhile, all the scintillator data and the fast Faraday cup data consistently show bunch durations of ≈ 2.5 ns.

Meanwhile, the spot size in these recent measurements is $\approx 2.1 \times$ smaller compared with Ref. [8]. Two significant changes to the experiment are the transverse focusing supplied by the 8-T final focusing solenoid and the modifications to the FCAPS described in Section 2.4. This is a significant improvement, though not as great as expected from PIC simulations assuming ideal neutralization. PIC simulations using the experimentally constrained plasma density distribution are underway which may lead to plasma injection modifications.

3. Further improvements

A number of beam manipulations and plasma source designs are under study, to improve the beam intensity on target for warm-dense matter experiments

Since mirroring of the plasma injected from outside the solenoid can limit the plasma density in the bore of the focusing element, we are exploring modification of the magnetic field topology near the target plane to allow more efficient plasma transport to the highest field region of solenoid while maintaining high plasma density near the target and in the fringe field of the solenoid. Modeling of plasma flow with auxiliary coils is underway. Also, more compact plasma sources are being designed.
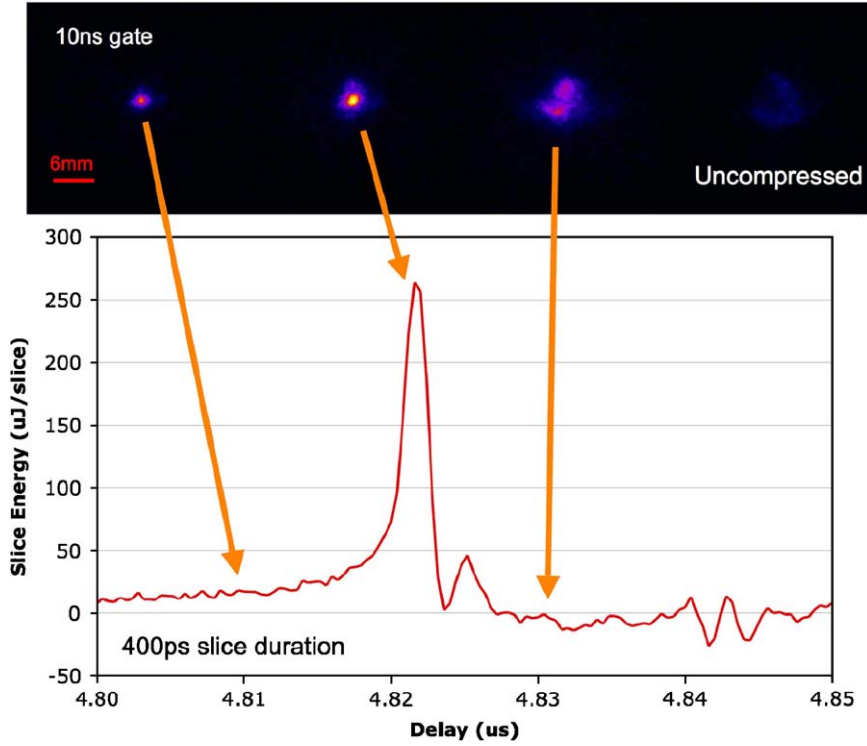
Fig. 7. Time-dependent transverse beam distributions demonstrating the simultaneous transverse focusing at the time of peak compression. The FWHM of the peak is ≈2.5 ns.

Smaller sources can be placed closer to the target plane, reducing the cross-field plasma transport.

We have recently constructed a new IBM. It has 20 induction core units (vs. the presently utilized 12 core units), or nearly twice the volt seconds (Vs) available compared with the present setup. The experiment design question is whether the increased capability should be used, for example, to impart a higher velocity tilt, $\Delta = \delta v / v_0$, (higher peak voltage), or keeping it unchanged for a shallower slope of the tilt and a correspondingly longer drift compression length.

The trade-offs are between a shorter focused pulse duration (with greater chromatic aberrations), or a longer pulse duration with fewer chromatic aberrations. The energy deposition on the target is approximately [16]:

$$E = \frac{4\phi I \tau}{\pi \varepsilon f \Delta} F_1(\eta) \tan^{-1}\left(\frac{F_2(\eta) r_0^2 \Delta}{2 f \varepsilon}\right) \propto \frac{\phi I \tau}{\varepsilon f \Delta} \tag{3}$$

where $e\phi$ is the ion kinetic energy, I is the beam current before compression, τ is the initial pulse duration before compression, ε is the un-normalized transverse emittance of the beam, f is the focal length of the final focusing solenoid, r_0 is the radius of the beam on entrance to the solenoid, and $F_1(\eta)$ and $F_2(\eta)$ are functions that depend only on the ratio η of the length of the solenoid to the focal length of the solenoid. (For NDCX1, $\eta = 0.43$, and $F_1(0.43) = 1.01$ and $F_2(0.43) = 1.24$.) Eq. (3) is based on assuming that all slices of the beam enter the solenoid at radius r_0 independent of velocity. Chromatic aberrations' influence on the spot radius is proportional to $(\Delta)^{1/2}$. Thus, keeping the focal length approximately the same in the experiment (attractive because of the simplicity), and increasing Δ and τ to use the additional Vs appear to cancel from the above scaling. Conversely, doubling the τ keeping Δ fixed, and doubling the drift compression distance (distance from the IBM gap to the target plane) approximately doubles E, and doubles the compressed pulse duration under the assumption of conservation of longitudinal emittance.

We tested these scaling arguments with a series of analytic approximations and LSP simulations which include several additional experimental constraints: (i) The range of initial beam envelope conditions at the entrance to the IBM is constrained by the beam pipe diameter and solenoid field strengths in the matching section. (ii) In addition to the desired velocity ramp, the IBM imparts a time-dependent defocusing in the transverse plane, dispersing the beam envelope at the entrance to the final focusing solenoid, compounding the chromatic aberrations. (iii) The initial conditions are also constrained by the beam pipe radius in the final focusing solenoid.

The analytic model is based on the formulae for the IBM waveform for a finite length, fully neutralized beam drift compressing to a longitudinal emittance-limited bunch. Transverse envelopes were calculated for multiple energy slices, using the KV envelope equation. The beam distributions for each energy slice, assumed to be Gaussian near the focal plane, were summed to estimate the peak E. An example of the transverse envelopes for multiple energy slices is shown in Fig. 8.

The sweeping of the focal plane about the desired location at $z = 572$ cm due to the energy dispersion is evident in Fig. 8.

The time-dependent velocity ramp, $v(t)$, which compresses the beam at a downstream distance L with a leading edge velocity $v(0)$, is

$$v(t) = \frac{v(0)}{(1 - v(0)t/L)}$$

and the IBM voltage waveform, $V(t)$, producing this ramp, applied in the envelope slice model as well as in the LSP simulations, is

$$eV(t) = \tfrac{1}{2}mv^2(t) - e\phi_0$$

$e\phi_0$ is the ion kinetic energy. Several calculations were carried out where τ and initial beam envelopes were varied parametrically in LSP and in the slice-envelope calculations. A few are highlighted in Table 2, which illustrate our observations and conclusions.
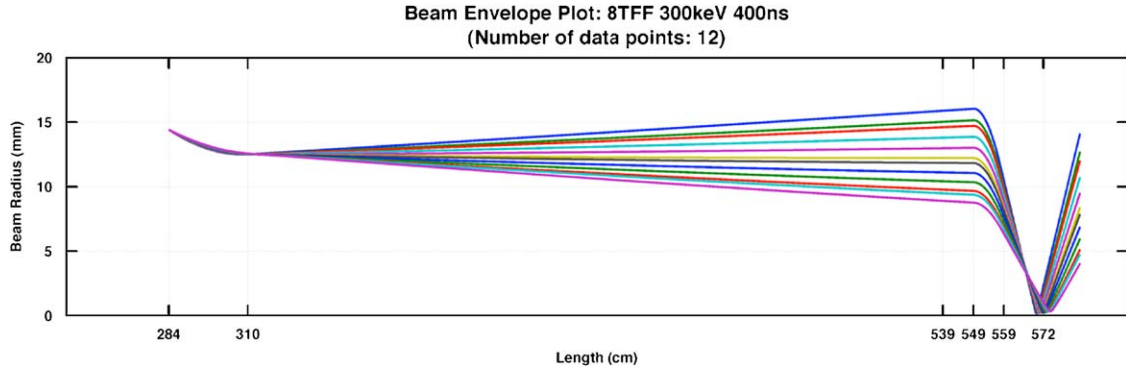
Fig. 8. The calculation is initialized at $z = 284$ cm, at the exit of the IBM gap. The envelope slices are calculated assuming full space-charge contribution, until the entrance to the FEPS at $z = 310$ cm. The beam propagates assuming full neutralization through the final focusing solenoid ($549 < z < 559$ cm) to the focal plane ($z = 572$ cm).

Table 2
Comparison of LSP, the envelope-slice model, and the simple analytic scaling relation (Eq. (3)).

	FF (T)	t (ns)	Initial kinetic energy (keV)	a ($z = 284$) (mm)	a' (mrad)	Current at focus (A)	Focus (ns)	E (J/cm^2) envelope	E (J/cm^2) LSP2	E (J/cm^2) (Eq. (1))
(a)	0	200	300	21.50	−23.80	3.08	1.69	0.06		
(b)	8	282	300	9.55	−9.82	4.01	1.83	0.39	0.30	0.59
(c)	8	400	300	14.40	−13.70	3.23	3.22	0.82	0.69	0.94

The first row (a) corresponds to experiments without a final focusing solenoid. The second and third rows correspond to beamlines using the new IBM, the final focusing solenoid ($B_{max} = 8$ T) and two beamline configurations: (b) with the present drift compression length ($L = 144$ cm), and (c) with twice the drift compression length ($L = 288$ cm) as the present setup.
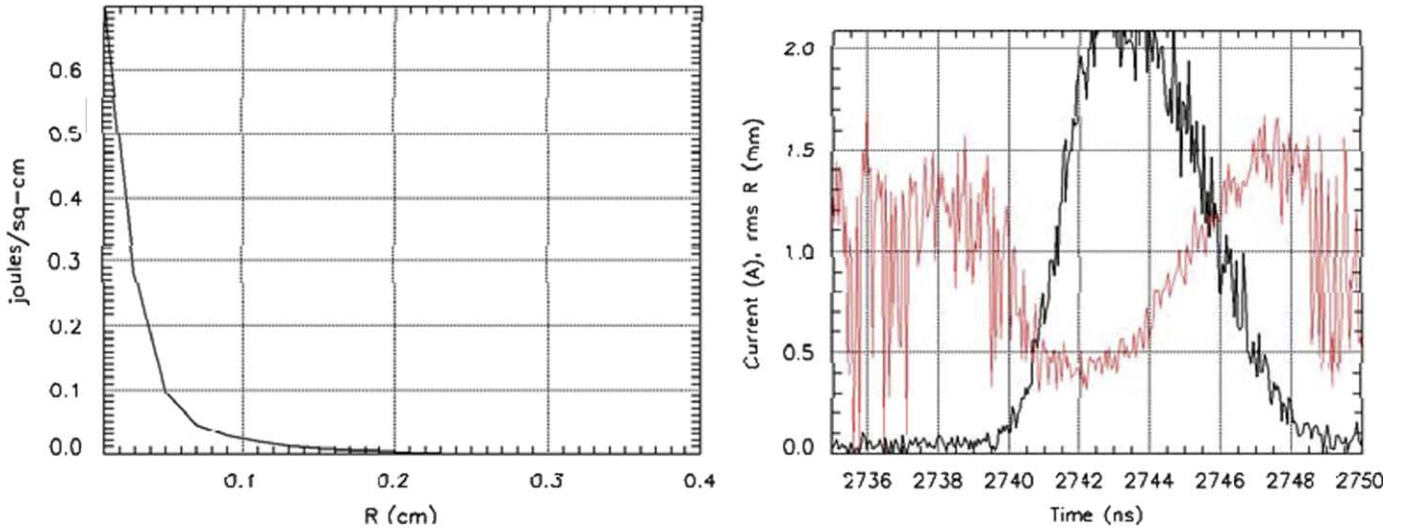

Fig. 9. LSP simulations predict a peak energy deposition of 0.69 J/cm^2 at the focal plane (left). In the right plot, the predicted peak current (black) is 2.1 A, with a minimum radius of 0.4 mm (red). The high-frequency oscillations are due to numerical noise (for interpretation of the references to colour in this figure legend, the reader is referred to the web version of this article).

We have noted that the overall magnitude of the energy deposition calculations is overestimated by the model calculations compared with NDCX data without a final focusing solenoid. For example, in case (a), the 2D LSP results are a factor of 3–4 greater than energy deposition observed in the experiment. This discrepancy is not yet resolved, but LSP simulations suggest that incomplete neutralization by the plasma and beam centroid offsets (which enhance the sampling of aberrations in the IBM fields) may be responsible.

It is clear that case (c) gives the highest energy deposition (0.69 J/cm^2) in the LSP simulations, $>2 \times$ greater than (b). This is at the expense of a longer pulse duration (3.2 ns FWHM), but satisfactory for initial warm-dense matter target experiments. The

LSP results for case (c) are shown in Fig. 9. Thus, we have concluded that it is advantageous to lengthen the drift compression section by 1.44 m via extension of the FEPS.

Time-dependent focusing to compensate for the large and otherwise limiting chromatic aberration in the bunched beam is desirable. For the near-term experiments, chromatic aberrations increase the rms focal spot size by about a factor of two. Applying the correction over a longer timescale is technically easier to achieve, thus the correction should be applied near the IBM. A first examination of requirements for a time-dependent lens indicates that a pulsed electric einzel lens or quadrupole doublet with relatively low potentials (10–20 kV) meet the requirements. A quadrupole triplet would allow correction of non-axisymmetric

rms-envelope parameters at injection to the bunching module to be brought to an axisymmetric distribution at the focal plane. This would increase the overall length of the correction element and will be studied in numerical simulations.

Acknowledgements

References

[1] J.J. Barnard, et al., Nucl. Instr. and Meth. A (2009), in press, doi:10.1016/j.nima.2009.03.221.
[2] S.A. MacLaren, et al., Phys. Plasmas 9 (5) (2002)
    D.V. Rose, et al., in: Proceedings of the Particle Accelerator Conference, Chicago, IL, 18–22 June 2001, IEEE, Piscataway, NJ, 2001, p. 3002.
[3] P.K. Roy, et al., Nucl. Instr. and Meth. A 544 (2005) 225;
    E. Henestroza, et al., PRST-AB 7 083501 (2004).
[4] P.K. Roy, et al., Phys. Rev. Lett. 95 (2005) 234801.
[5] P.C. Efthimion, et al., in: Proceedings of the Particle Accelerator Conference, Knoxville, ⟨http://accelconf.web.cern.ch/AccelConf/p07/PAPERS/THPAS082.PDF⟩, 2007.
[6] D.R. Welch, D.V. Rose, B.V. Oliver, R.E. Clark, Nucl. Instr. and Meth. A 464 (2001) 134.
[7] D.R. Welch, et al., Nucl. Instr. and Meth. A 577 (2007) 231.
[8] J.E. Coleman, et al., in: Proceedings of the Particle Accelerator Conference, Albuquerque, NM, June 25–29 (IEEE catalog# 07CH37866, USA, 2007), ⟨http://accelconf.web.cern.ch/accelconf/p07/PAPERS/THPAS004.PDF⟩, 2007, pp. 3516–3518.
[9] A.B. Sefkow, R.C. Davidson, Phys. Rev. ST Accel. Beams 10 (2007) 100101 and references therein.
[10] F.M. Bieniosek, et al., Nucl. Instr. and Meth. A (2009), in press, doi:10.1016/j.nima.2009.03.123.
[11] A.B. Sefkow, et al., Phys. Rev. ST Accel. Beams 9 (2006) 052801 ⟨http://prst-ab.aps.org/pdf/PRSTAB/v9/i5/e052801⟩.
[12] R.H. Cohen, et al., Nucl. Instr. and Meth. A (2009), in press, doi:10.1016/j.nima.2009.03.083.
[13] F.M. Bieniosek, et al., Nucl. Instr. and Meth. A 544 (2005) 268 (Proceedings of the 15th International Symposium on Heavy Ion Inertial Fusion HIF, 2004).
[14] F.M. Bieniosek, M. Leitner, in: Proceedings of the 22nd Particle Accelerator Conference, Albuquerque, NM, June 25–29 (IEEE catalog# 07CH37866, USA, 2007), ⟨http://cern.ch/AccelConf/p07/PAPERS/FRPMS018.PDF⟩, 2007, pp. 3940–3942.
    J.E. Coleman, Intense ion beams for warm dense matter physics, Ph.D. Thesis, University of California, Berkeley, 2008.
[15] P.K. Roy, et al., Nucl. Instr. and Meth. A (2009), in press, doi:10.1016/j.nima.2009.03.228.
[16] J.J. Barnard, et al., in: Proceedings of the Particle Accelerator Conference, Knoxville, Tennessee, ⟨http://cern.ch/AccelConf/p05/PAPERS/RPAP039.PDF⟩, 2005.